Available online at www.sciencedirect.com
SCIENCE DIRECT®
Journal of Catalysis 223 (2004) 395–403
JOURNAL OF CATALYSIS
www.elsevier.com/locate/jcat

# Structure of vanadium oxide supported on mesoporous carbon-coated monoliths and relationship with its catalytic performance in the SCR of NO at low temperatures

E. García-Bordejé,[a,*] M.J. Lázaro,[a] R. Moliner,[a] J.F. Galindo,[b,1] J. Sotres,[c,1] and A.M. Baró [b,1]

[a] *Instituto de Carboquímica (CSIC), Miguel Luesma Castán 4, 50015 Zaragoza, Spain*
[b] *Universidad Autónoma de Madrid, Dep. Física de la Materia Condensada C-III, 28049 Madrid, Spain*
[c] *Nanotec Electrónica S.L., Pabellón C, Campus Cantoblanco, 28049 Madrid, Spain*

Received 21 January 2004; revised 13 February 2004; accepted 17 February 2004

**Abstract**

A novel monolithic catalyst based on vanadium supported on mesoporous carbon has been prepared. Vanadium has been supported on carbon-coated monoliths with four different loadings, viz. 3, 4, 6, and 8 wt%. The structure of vanadium catalyst has been characterized by atomic force microscopy (AFM), $N_2$ adsorption, and XRD. All these techniques indicate that vanadium is dispersed as overlayers up to 6 wt% loadings. For higher loadings crystallites appear. The size of these crystallites (12 nm average height) has been characterized by AFM. The catalysts prepared have been tested in the SCR of NO at low temperatures (363–453 K). Similar activities and selectivities to $N_2$ were found up to monolayer coverage. Above monolayer coverage activity and selectivity diminish dramatically. The catalysts prepared here show activity and selectivity comparable to those of the most active catalysts reported in the literature. Furthermore, the monolithic shape endows it with significant advantages over the fixed bed.


*Keywords:* Vanadium oxide catalyst; Carbon-coated monoliths; SCR of NO; Atomic force microscopy

## 1. Introduction

Vanadium oxide has unique redox and acid base properties. As a result, V-containing catalysts have been extensively used in a large number of catalytic processes involving selective oxidation reactions (such as conversion of butane to maleic anhydride, oxidation of *o*-xylene, 1,3-butadiene, methanol, and CO, ammoxidation of hydrocarbons, selective catalytic reduction of NO, and partial oxidation of methane) [1–4].

The catalyst used in industrial practice is normally supported on metal oxides, e.g., $TiO_2$, $Al_2O_3$, $ZrO_2$, and $SiO_2$. Supporting a metal oxide on the surface of another oxide was initially proposed to improve the catalytic activity of the active metal oxide phase due to a gain in surface area and mechanical strength. The molecular structures and morphologies of vanadium supported on these oxides have been intensively studied [5–10]. These studies have revealed that the geometric and electronic structure of surface vanadium oxides is the fundamental basis for the catalytic performance. There is a general consensus that structural and reactivity characteristics of vanadium oxide are modified with respect to bulk vanadium oxide by interaction with the oxide support surface and that this specific oxide–oxide interaction leads to a spreading of vanadium oxide over the support surface to form a thin monolayer film. The dispersion depends on the available surface area as well as the availability of surface hydroxyl groups. Hence, the surface population of hydroxyl sites determines the monolayer coverage of the supported oxide. Monolayer coverage is defined as the maximum loading at which the supported oxide is deposited as surface species, free of tridimensional aggregates. In this sense, "monolayer" surface coverage of vanadia overlayer on oxide support was determined to be approximately 7–8 $VO_x$ per $nm^2$ [1].

In the preparation of these catalysts upon calcination, the formed dehydrated vanadium oxides directly anchor to the surface via an esterification reaction with the hy-

* Corresponding author.
*E-mail address:* jegarcia@carbon.icb.csic.es (E. García-Bordejé).
[1] On leave at the Instituto de Carboquímica (CSIC), Zaragoza.

0021-9517/$ – see front matter 
doi:10.1016/j.jcat.2004.02.018

droxyl groups of the support, resulting in the formation of surface vanadium oxides. Spectroscopic studies of $VO_x$ supported on different metal oxides showed the coexistence of $V_2O_5$ crystallites and species which have V–O–V bonds [8–10]. Four kinds of $VO_x$ species are proposed for supported $VO_x$: (a) isolated species (orthovanadate); (b) dimeric (pyrovanadate) or polymeric species, this polymeric species can also form chains of vanadium ions building up two-dimensional overlayers; (c) $VO_x$ three-dimensional thin overlayers; (d) $V_2O_5$ crystallites.

Much more scarce is the literature dealing with the characterization of the structures of vanadium supported on carbon support, despite that this catalyst has shown recently very good performance in the selective catalytic reduction of $NO_x$ at low temperatures [11–16]. The limited use of carbon can be based on the general belief that the interaction of the active phase with carbon is weaker than with an oxide support, thus leading to lower dispersions. However, this is not completely true because the surface chemistry of activated carbon can be tuned to create hydroxyl groups and, moreover, the surface area is much higher than in the metal oxide supports.

Selective catalytic reduction (SCR) of NO with ammonia in the presence of oxygen is the proven technology for the effective removal of $NO_x$ from stationary sources [17]. A catalyst based on $V_2O_5/TiO_2$ with and without the addition of either $WO_3$ or $MoO_3$ was developed and successfully commercialized for $NO_x$ removal at 350–400 °C [18,19]. However, the high concentration of $SO_2$ and ash, e.g., $K_2O$, CaO, and $As_2O_3$, in the flue gas reduces their performance and longevity. To circumvent this problem an attractive option is to place the SCR unit downstream of the desulfurization and electrostatic precipitators where most $SO_2$ and ash have been removed. Even after the desulfurization around 100–1000 ppm $SO_2$ remains. Since the temperature in the downstream is typically below 200 °C, it is necessary to develop low-temperature SCR catalysts to avoid reheating of the flue gas and thus decreasing the cost of the process. To meet this aim, catalysts supported on carbon have shown very high activity at low temperatures and resistance to the remaining $SO_2$ [11–16,20–24]. To the best of our knowledge none of these authors studies in detail the relationship between the structure of the catalyst and its performance in reaction.

In this work, cordierite monoliths have been coated with mesoporous carbon derived from the blend of two polymers. Subsequently, different vanadium loadings have been supported on carbon-coated monoliths. The structure of vanadium has been characterized by several techniques, viz. atomic force microscopy, $N_2$ adsorption, and XRD. The catalysts prepared have been tested in the SCR of NO at low temperatures (363–453 K). One of the objectives of characterization is determining the loading at which vanadium is dispersed on the carbon support as monolayer. The results enabled us to unravel the relationship between the structure of this novel system, i.e., vanadium/carbon-coated monoliths, and its catalytic activity and selectivity. Furthermore, a comparison has been made between vanadium supported on this carbon and on other traditional oxide supports.

## 2. Experimental

### 2.1. Preparation of carbon-coated monoliths

Cordierite monoliths (400 cpsi, 1 cm diameter, 5 cm length) were coated with a polymer blend by the method described elsewhere [16,25,26]. The polymers used are Furan resin (Huttenes-Albertus) and polyethylene glycol-6000 mol wt (Sigma-Aldrich). After thermal curing, the monoliths were carbonized at 973 K, activated with $CO_2$ at 1173 K for 8 h (30% carbon burn-off), and treated for 24 h with $HNO_3$ 1 N at room temperature to create oxygenated surface groups.

### 2.2. Vanadium catalyst preparation

The carbons prepared were loaded with different amounts of vanadium, i.e., 3, 4, 6, and 8 wt%. The impregnation was carried out by equilibrium adsorption of ammonium metavanadate in the stoichiometric amount to get the desired vanadium loading on carbon. To facilitate the dilution of ammonium metavanadate ca. 10 mg of oxalic acid was added. Under these conditions the pH of solution remains neutral and the solution holds a yellow color indicative of the presence of $VO_2^+$.

The monoliths placed in a holder were introduced in a vessel with 100 ml of the impregnating solution. The vessel has a stirrer at the bottom that creates a continuous flux of the vanadium solution through the monoliths. This guarantees that vanadium is deposited inside the channels. This process was allowed to proceed for 18 h. It was visually observed that the solution turns from a yellow color to colorless in a few hours indicating that all vanadium in solution has been adsorbed. After this process the monoliths were rinsed with distilled water in the same setup. The V content of the solutions before and after impregnation was analyzed by ICP. From the difference in V content of these solutions the V loading was calculated. Finally, the catalyst was calcined in Ar at 673 K.

### 2.3. Characterization of vanadium catalyst

In order to characterize the topography of the samples we used atomic force microscopy. The images were recorded with a commercial system from Nanotec Electrónica S.L. The AFM was operated in the dynamic mode, where the cantilever is oscillated at its eigenfrequency (72 kHz) and feedback is adjusted in order that there is no contact between the sample and the tip. In addition to the topographic image, we also collected the phase-shift image. Phase-shift data can be collected simultaneously with height data. Phase-shift detection measures the phase lag between the drive signal

and the actual tip response signal. In phase-shift detection, the contrast mechanism is a convolution of topography and material/chemical properties of the surface. This allows distinguishing between the vanadium and the carbon substrate due to their different chemical composition.

The vanadium particle dimensions were determined by analysis of the height AFM images collected using the software supplied by WSxM. Section analysis provides a cross-sectional height profile of the surface along a reference line, which is drawn across the region of interest. This permits accurate estimation of the vertical dimensions of the surface features. Lateral dimensions of particles in this size range can be exaggerated by finite tip radius effects. More than 35 images of every sample were recorded, some of them being featureless.

Nitrogen adsorption was performed on a Quantachrome Autosorb-1 at 77 K. The pore volume and pore-size distribution were calculated using the BET method. From the physisorption measurements with nitrogen the specific surface area has been calculated by the BET (Brunauer, Emmet, and Teller) theory in the relative pressure range 0.01–0.10 following standard ASTM-4365, which is applicable to microporous materials. The *t* plot method was applied to calculate the micropore volume and micropore surface area. Pore-size distribution was obtained from the desorption branch of the $N_2$ isotherm according to the BJH method.

X-ray diffraction (XRD) patterns were recorded using a Philips PW 1840 diffractometer using nickel-filtered Cu-$K_\alpha$ radiation.

### 2.4. Catalytic tests

The catalysts prepared were tested in the selective catalytic reduction of NO with ammonia at four temperatures, viz. 363, 393, 423, and 453 K. The gas composition was 700 ppm NO, 800 ppm $NH_3$, 3% $O_2$, and balance Ar. The catalytic tests were performed in a quartz reactor in which two cylindrical monoliths (1 cm diameter, 5 cm length) were placed in parallel. The gas was forced to flow through the monolith channels by fixing the monoliths to the inner walls of the reactor using Teflon stripe. The total amount of carbon coating was ca. 0.3 g and the total flow rate was 100 ml/min STP that yields a GHSV $\sim 17{,}000\ h^{-1}$. Under these conditions the maximum observed reaction rates lies in the range of kinetic control, with no diffusion control (internal, external, or axial) according to the standard criteria [27,28].

To analyze the gases a mass spectrometer (Balzers) was used. The mass spectrometer was calibrated with cylinders of gases with known composition. The following main mass-to-charge ($m/e$) ratios were used to monitor the concentration of products and reactants: 17 ($NH_3$), 18 ($H_2O$), 28 ($N_2$), 30 (NO), 32 ($O_2$), 44 ($N_2O$), and 46 ($NO_2$). The fragmentation pattern of each gas was dealt with as follows. From the mass $m/e$ 12 and taking into account that the contribution of $CO_2$ to $m/e$ 12 is 6%, the amount of $CO_2$ desorbed at steady state has been calculated. The $N_2O$ concentration has been calculated from $m/e$ 44 after subtracting the contribution of $CO_2$. The NO concentration has been calculated from $m/e$ 30 subtracting the contribution to this mass of $N_2O$ (30%). The concentration of $N_2$ has been calculated from $m/e$ 28 subtracting the contribution of $N_2O$ (11%) and $CO_2$ (11%). Finally the $NH_3$ concentration has been obtained from $m/e$ 17.

From the concentration of the gases at steady state both the conversion and the selectivity are calculated according to

$$\text{Conversion} = \frac{[\text{NO}]_{\text{in}} - [\text{NO}]_{\text{st}}}{[\text{NO}]_{\text{in}}} \times 100, \tag{1}$$

$$\text{Selectivity} = \frac{[\text{N}_2]_{\text{st}}}{[\text{N}_2]_{\text{st}} + [\text{N}_2\text{O}]_{\text{st}}} \times 100. \tag{2}$$

The subscripts in and st stand for the inlet concentration and outlet concentration at steady state, respectively. All experiments were repeated and the maximum difference between the results was 1% of the value, indicating that the catalyst is not deactivated.

## 3. Results

In the preparation of supported catalysts by impregnation, the sorption of metal ions in solution is influenced the physical-chemical properties of the support, pH of impregnation, and nature of the solvent. When the pH of impregnating solution is higher than the point of zero charge (PZC), the surface of the support will become negatively charged, and the adsorption of cations is favored [29]. The main goal of the oxidation with $HNO_3$ is to obtain a more hydrophilic surface with a relatively large number of oxygen-containing surface groups, hence decreasing the PZC. In our case the PZC of the carbon treated with $HNO_3$ is around 3 and the pH of the solution is higher (neutral) that favors the adsorption of the cation ($VO_2^+$) on the negatively charged oxygenated surface groups. This is confirmed by the rapid decoloration of the yellow vanadium solution. These groups are located in the edges and defects of the basal planes and in the micropores. Accordingly, the vanadium ions will be anchored on these sites. Furthermore, the groups created after the oxidation with $HNO_3$ contribute to evenly disperse the vanadium along the length of the monolith. The even distribution of vanadium along the monolith was verified by cutting the monolith in three parts and analyzing the vanadium content by ICP. The vanadium content in each part was very similar and equivalent to the nominal vanadium content.

### 3.1. Catalyst characterization

Fig. 1 shows a peculiar AFM image with four very regular features found in sample with 8 wt% vanadium. Fig. 1a is the topographical image and Fig. 1b is the phase-shift image. The different contrast between the features and the support in the phase-shift image enables us to state that the features in the picture have a different chemical composition than the

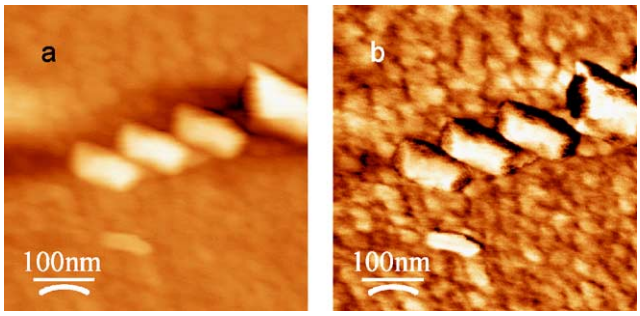


Fig. 1. AFM image showing four neighboring vanadium crystallites in a sample with 8 wt% vanadium. (a) Topographic image; (b) phase-shift image that allows the different chemical natures of the crystallites and the support to be distinguished.

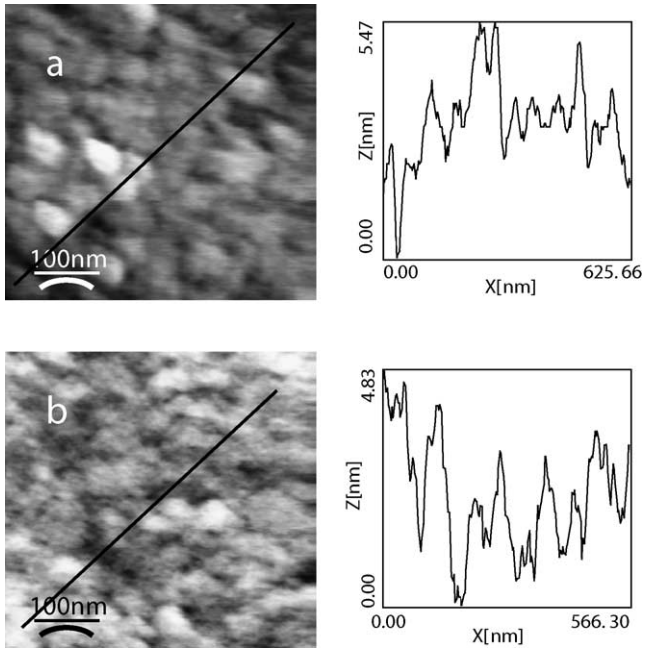


Fig. 2. AFM images representative of (a) support, (b) samples with 3 and 4 wt% vanadium. Left, AFM top view; right, profile along the line in the top view.

carbon support; i.e., these crystallites can be unambiguously ascribed to vanadium. Figs. 2–4 show some AFM pictures pertaining to each vanadium loading. At the left there is a top view image and at the right there is the profile in nanometers along the line drawn in the top view. It is important to note that AFM is a technique than only allows seeing features in the external surface, thereby it is blind to catalyst particles in the pores. Also it is not possible to characterize vanadia aggregates smaller than 4 nm since they cannot be discerned from the roughness of the support. Fig. 2a shows a standard image of the carbon support and Fig. 2b is an image representative of samples with 3 and 4 wt% vanadium. No apparent crystallites were observed in any image of sample with 3, 4 wt% V (Fig. 2b). This image resembles that of the carbon-coated support (Fig. 2a). In sample with 6 wt% V, 35 images were recorded and only 4 images showed some small

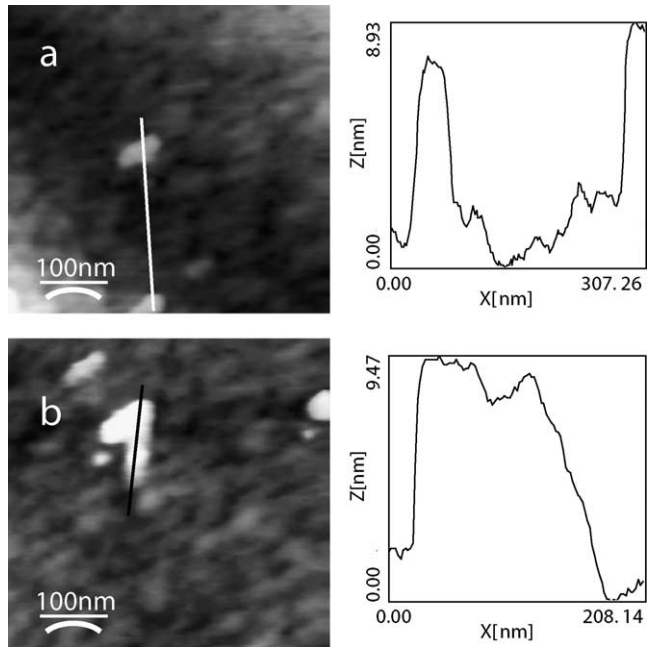


Fig. 3. Pictures of samples with 6 wt% of vanadium with some isolated features. Only 4 of the 35 images recorded showed some features (average height 7 nm). Left, AFM top view; right, profile along the line in the top view.

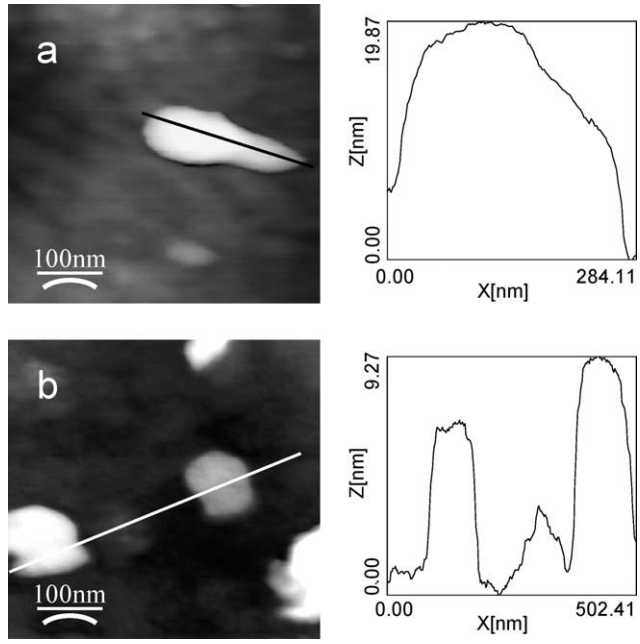


Fig. 4. Pictures of samples with 8 wt% vanadium with the typical crystallites observed in this sample. Left, AFM top view; right, profile along the line in the top view.

features. Figs. 3a and b correspond to two of the pictures of sample 6 wt% V with features. These small features have a height around 7 nm. It is apparent that most of vanadium in sample with 6 wt% V is not detectable by AFM because either it is inside the pores or it has height smaller than 4 nm or both.

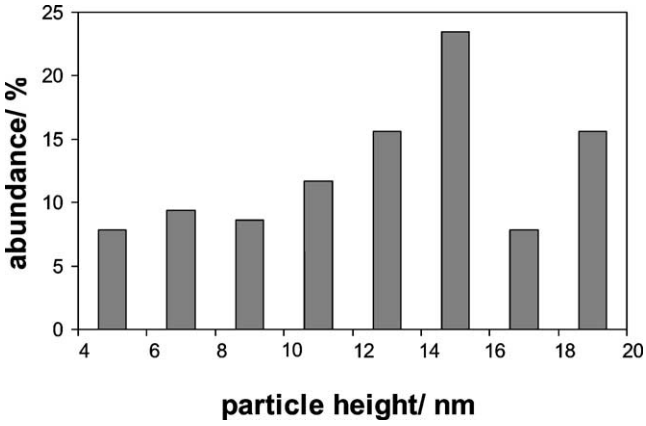


Fig. 5. Particle height distribution of crystallites detected by AFM in carbon-coated monoliths with 8 wt% vanadium. Twenty-five crystallites were used in this particle height distribution.

Table 1
Average RMS roughness obtained by the treatment of images by digital software

| V loading (wt%) | 0 | 3 | 4 | 6 | 8 |
|---|---|---|---|---|---|
| Average RMS roughness (nm) | $2.5 \pm 0.05$ | $1.5 \pm 0.04$ | $1.4 \pm 0.03$ | $2.0 \pm 0.04$ | $3.5 \pm 0.05$ |

Fig. 4 illustrates two images representative of sample with 8 wt% vanadium. In this sample 35 images were recorded, 27 of them showing some crystallites. All these crystallites have some common features; viz. they are flat at the top and they are located at the entrance of macropores or depressions of the support (darkest color in the pictures). The flatness of the top agrees with the laminar structure of $V_2O_5$ crystals reported in the literature [30,31]. The borders of pores correspond to the edges of carbon basal planes where there is a high density of oxygenated surface groups that act as anchoring sites for vanadia precursor. Therefore, it is not surprising that the crystallites are located near the entrance of pores. Moreover, the steps or depressions in the surface can serve to stabilize $V_2O_5$ crystallites during the growing process. The crystallite height distribution of sample 8 wt% is displayed in Fig. 5. The average particle height was 12 nm and the lateral dimensions ranged 130-170.

From the digital treatment of images the values of average RMS roughness were calculated and they are displayed in Table 1. The average RMS roughness increases with vanadium loading. This is a consequence of the increase of number and size of the features. It is also observed that the average RMS roughness of the sample with 3 and 4 wt% vanadium decreases with respect to that of the support. A possible interpretation is that vanadium oxide is deposited as a layer in the mesopore walls decreasing their diameter. This would render an apparently smoother surface because some mesopores mouths become inaccessible to the AFM tip.

The textural characterization by $N_2$ adsorption revealed that the samples are micro and mesoporous. Table 2 shows the values of the pore volume and surface area both of micro- and mesopores. In a comparison of the textural features of the samples loaded with different percentages of vanadium with those of the support, the total pore volume and area remain practically unchanged up to 6 wt% loading. Hence, there is no pore clogging. The exception is sample loaded with 8 wt% V where there is a significant decrease of the surface area and pore volume both in the micro and mesoporous range. The decrease in surface area is more relevant in the case of microporosity. This occurs because the big crystallites detected by AFM can plug some micro- and mesopores. In the case of the samples loaded with 3, 4, and 6 wt% of vanadium the total surface area and pore volume apparently do not change but intriguingly the micropore volume and surface area increase in detriment of the mesopore volume and area. This can support again the fact that a layer of vanadium covers the narrow mesopore walls. Hence these mesopores decrease their diameter, becoming micropores.

The results described above were also confirmed by XRD. The diffraction peaks of $V_2O_5$ were only found in catalyst with vanadium loading of 8 wt% (not shown) indicating that the dispersion on this latter catalyst is poorer than in the former ones. It was not possible to determine the particle size out of these XRD peaks since they are very small and broad.

### 3.2. Testing in the SCR of NO at low temperatures

To ascertain the effect of vanadium loading in the activity, the kinetic rate constants per catalyst weight ($k_c$) and per vanadium weight ($k_m$) have been calculated. For oxygen partial pressures over 1% atm, the SCR reaction can be considered to be approximately first order with respect to NO and zero order with respect to $NH_3$. As noted above, the reaction was found to be free of diffusional limitations. Under these conditions the apparent rate constant ($k$) and the NO

Table 2
Textural parameters by $N_2$ adsorption

| V loading (%) | Nominal $VO_x$ surface density ($V\,nm^{-2}$) | BET area ($m^2\,g^{-1}$) | Total pore volume ($cc\,g^{-1}$) | Micropore area ($m^2\,g^{-1}$) | Mesopore area ($m^2\,g^{-1}$) | Micropore volume ($cc\,g^{-1}$) | Mesopore volume ($cc\,g^{-1}$) |
|---|---|---|---|---|---|---|---|
| 0 | 0 | 617 | 0.96 | 326 | 292 | 0.18 | 0.78 |
| 3 | 0.57 | 620 | 0.84 | 397 | 223 | 0.23 | 0.61 |
| 4 | 0.75 | 629 | 0.86 | 402 | 227 | 0.23 | 0.63 |
| 6 | 1.17 | 607 | 0.90 | 354 | 253 | 0.20 | 0.70 |
| 8 | 1.78 | 529 | 0.77 | 259 | 270 | 0.16 | 0.61 |

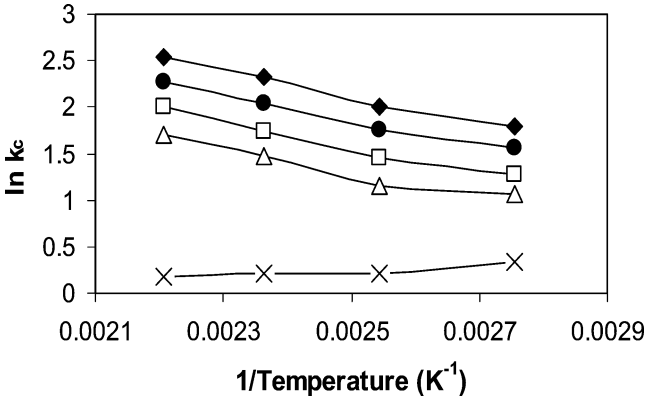


Fig. 6. Arrhenius plot ($\ln k_c$ vs $1/T$) for the different vanadium loadings: (×) carbon support, (△) 3 wt%, (□) 4 wt%, (◆) 6 wt%, and (●) 8 wt%. The Arrhenius parameters have been calculated from the straight part, i.e., temperatures 393, 423, and 453 K.

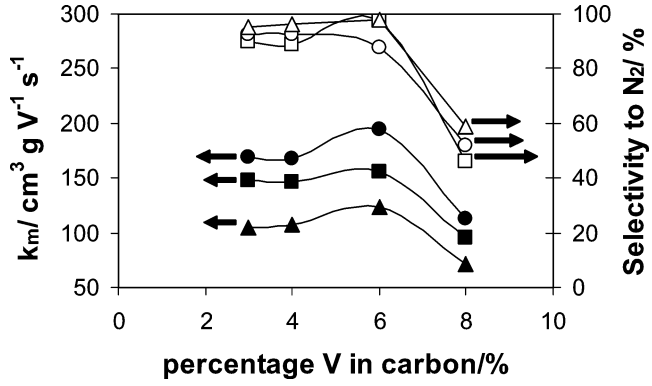


Fig. 7. Testing of the catalysts in the SCR of NO at three temperatures. Kinetic rate constant per vanadium weight ($k_m$): (▲) 393 K, (■) 423 K, and (●) 453 K; selectivity to $N_2$: (△) 393 K, (□) 423 K, and (○) 453 K.

conversion ($X$) are related as follows,

$$k = -\frac{F_0}{[\mathrm{NO}]_0 W}\ln(1-X), \tag{3}$$

where $F_0$ is the molar NO feed rate (mol/s), $[\mathrm{NO}]_0$ is the molar NO concentration at the inlet (mol/cm$^3$), and $W$ is either the weight of catalyst ($k_c$) or the weight of vanadium loaded ($k_m$).

Fig. 6 shows the Arrhenius plot, i.e., $\ln k_c$ vs $1/T$. The plot is a straight line at the three highest temperatures. From this straight line the apparent activation energies and preexponential factors have been calculated. These are reported in Table 3 along with the values of $k_c$ and $k_m$ at 423 K. At the lowest temperature (363 K) the slope is less steep because at this temperature the process of NO adsorption prevails over the catalytic one. The activation energy is almost constant for all V loadings. This activation energy is lower than the intrinsic activation energies reported for the SCR at high temperatures [32]. But it is comparable to the apparent activation energies for the SCR al low temperatures reported by several authors [33,34]. According to these authors the SCR reaction at low temperatures takes place following a Langmuir–Hinshelwood mechanism. Hence the low overall activation energy is due to the exothermal contributions of the elementary steps of NO adsorption and site reoxidation.

Fig. 7 shows the values of $k_m$ and the selectivity to $N_2$ at several temperatures for the monolithic catalyst prepared in this work. It is apparent that the rate constants increase slightly up to 6 wt% loading and then drops in the sample with 8 wt% vanadium. These kinetic rate constants are comparable to those of the most active catalysts reported in the literature for the SCR of NO at low temperature [16]. The selectivities to $N_2$ are around 90% up to 6 wt% loading and then declines to ca. 50% for sample with 8 wt% vanadium. The increase of temperature leads to an increase of the kinetic rate constant but the temperature does not have a clear influence on selectivity.

To compare the specific activity of our catalyst with that of vanadia on other supports reported in the literature, the turnover frequency was calculated assuming a first-order reaction rate [Eq. (4)]. The turnover is defined as the number of moles of NO converted per mole of vanadium atom per second.

$$\mathrm{TOF} = -\frac{F_0}{M}\ln(1-X), \tag{4}$$

where $F_0$ is the molar NO feed rate (mol/s), $M$ is the moles of vanadium, and $X$ is the conversion. The TOF values at 423 K of the catalyst here prepared are displayed in Table 3. It is observed that the turnover is approximately the same for submonolayer coverages.

In order to examine the stability of the catalyst with time on stream, all catalysts were essayed during 15 h TOS at 423 K. In these tests, the activity and selectivity remained without variation. In the SCR experiments at 393 and 423 K the amount of $CO_2$ evolved amounts to less than 50 and 70 ppm, respectively. At 453 K a kind of onset on carbon gasification is observed and $CO_2$ amounts to 300 ppm. In general the carbon support is very stable, especially at the lowest temperatures.

## 4. Discussion

In samples with 3, 4, and 6 wt% V almost no features ascribable to crystallites were found by AFM. This points out that most of the vanadium is in a dispersed fashion as isolated species, polymeric chains, or overlayers. This is also supported by the results of $N_2$ adsorption, because there is no pore plugging and the mesopores reduce their diameter, indicating that layers of vanadium are covering their walls. On the contrary, in a sample with 8 wt% V, the crystallites found in AFM images, the diffraction peaks of $V_2O_5$, and the decrease in pore volume indicate that the predominant species is vanadia crystallites. Accordingly, the monolayer coverage in this vanadium/carbon catalyst, defined as maximum loading at which vanadium is dispersed before three-dimensional aggregates start to grow, is ca. 6 wt% vanadium.

From the catalytic experiments a relationship between the structure of vanadium and the catalytic behavior arises. The

Table 3
Kinetic rate constants, turnover frequencies, and parameters of Arrhenius equation

| Catalyst | $k_c$ at 423 K ($cc\,s^{-1}\,g^{-1}$) | $k_o$ ($cc\,s^{-1}\,g^{-1}$) | $E_a$ ($kJ\,mol^{-1}$) | $k_m$ at 423 K ($cc\,s^{-1}\,g^{-1}$) | TOF at 423 K (mol NO (mol $V^{5+}$)$^{-1}$ $s^{-1}$) |
|---|---|---|---|---|---|
| 3% V | 4.3 | 227.9 | 13.9 | 144.5 | $1.6\times10^{-4}$ |
| 4% V | 5.9 | 292.6 | 13.8 | 146.7 | $1.7\times10^{-4}$ |
| 6% V | 9.4 | 422.8 | 13.2 | 156.5 | $1.8\times10^{-4}$ |
| 8% V | 7.7 | 295.9 | 12.8 | 95.8 | $1\times10^{-4}$ |

Table 4
Comparison of TOF values at low temperatures of the carbon-supported catalyst prepared in this work and vanadia supported on other supports

| Catalyst ID number | V content (% (w/w)) | Support | Temperature (K) | TOF (mol NO (mol $V^{5+}$)$^{-1}$ $s^{-1}\times10^{-4}$) | Reference |
|---|---|---|---|---|---|
| 1 | 0.6 | $TiO_2$ | 473 | 2.7 | [5] |
| 2 | 0.82 | $TiO_2$ | 500 | 2 | [40] |
| 3 | 0.6 | $Al_2O_3$ | 473 | 0.8 | [5] |
| 4 | 0.6 | $SiO_2$ | 473 | 1 | [5] |
| 5 | 8.4 | $Al_2O_3$ | 423 | 1.7 | [41] |
| 6 | 1.9 | $TiO_2$ | 423 | 3.5 | [42] |
| 7 | 3.36 | $TiO_2$ | 473 | 16 | [5] |
| 8 | 6 | Carbon | 423 | 1.8 | This work |

kinetic rate constant relative to vanadium weight ($k_m$) are approximately constant in samples 3, 4, and 6 wt% V, i.e., up to monolayer coverage. $k_m$ increases 7% in sample 6 wt% V but this increase is not significant because it is within the experimental error. The activity drop in 8 wt% sample can be explained because all vanadium is not active in the crystallites, but only vanadium at the surface which is exposed to the gas phase. Furthermore, the decrease in BET surface area of this sample suggests that some vanadium can be buried in the micropores. The dramatic decrease of selectivity in this sample agrees with the results of Ozkan et al. [37]. These authors studied the SCR reaction with vanadia crystals having a preferential exposure of different crystal planes. They found that the product distribution varies with the exposed crystal plane and V=O sites promote both nitrous oxide formation from $NO + NH_3$ and from direct oxidation of ammonia. Therefore in the crystallites observed in samples with 8 wt% vanadium different crystal planes coexist, some of them catalyzing the production of $N_2O$.

From all the above, the dispersion of vanadium is crucial for both the efficiency and the selectivity of the catalyst. This is consistent with most of the results in the literature for the SCR of NO at high temperatures in which vanadium is supported on metal oxide [5,35,36,38–42]. All these authors emphasize the necessity of well-dispersed vanadium overlayers, irrespective if they propose a mechanism in which the bond involved in the reaction is the V=O [35,36], the V–O–V [19], or the V–O–support bond [1,5].

In a literature revision about vanadia supported on supports other than carbon, it was difficult to find activity data at low temperatures. Most experiments are performed at temperatures above 473 K. This is due, among other things, to the known instability of titania-supported vanadia at low temperatures. This instability arises from the poisoning with ammonium sulfate salts whose fusion temperature is 453 K. Table 4 shows the TOF values of the few references found in the literature dealing with the testing of vanadium supported on metal oxides at temperatures lower than 500 K. When comparing the catalyst here prepared with low loaded catalysts (catalysts 1–4) some conclusions can be drawn. It is apparent that the catalyst prepared here has TOF values similar (catalyst 2) or a factor of 0.7 lower (catalyst 1) than $TiO_2$-supported catalyst. However, the TOF value of our catalyst is a factor of 2 higher than that of vanadia supported on $Al_2O_3$ and on $SiO_2$ (catalysts 3 and 4). From all this, it appears that the metal–support interaction plays an important role on the specific activity of supported vanadia. This has led the authors to think that the V–O–support bond is relevant for SCR reaction in agreement with Wachs et al. [5]. Hence the turnover is directly related to the lability of this oxygen at the temperature of reaction. The lability of this bond would follow this trend $TiO_2 \geqslant$ carbon $> SiO_2 \approx Al_2O_3$.

Different is the case when we compare the carbon-supported catalyst prepared here with the high loaded samples on other supports (catalysts 5–7). The TOF of $Al_2O_3$-supported vanadia (catalyst 5) reaches the TOF value of our catalyst while the $TiO_2$-supported catalyst (catalyst 7) overtakes our catalyst in one order of magnitude. In the literature, this increase of TOF with the loading is attributed either to the higher activity of polymerized species [5,42] or to the necessity of two adjacent redox and acid sites for the reaction [36,41]. In contrast, the specific activity (TOF) of our catalyst does not depend on the vanadium loading as shown in Fig. 7 and Table 3. This indicates that the active phase does not change with the loading, i.e., either the V–O–V bond is irrelevant for the reaction or there is no polymerization of vanadia. This latter could be tentatively explained because carbon has a relative high surface area with low density of

hydroxyl groups. This renders a surface with relatively low density of vanadia. Consequently, the polymerization is less likely to occur than in other supports with lower surface areas and higher densities of hydroxyl groups. A possibility that remains to be explored is the use of characterization techniques which can give more information about the structure of dispersed vanadia species as, e.g., XPS.

Although the specific activity at monolayer coverage of $TiO_2$-supported catalyst is higher than that of our carbon-supported catalyst, carbon has some advantages over titania in the SCR of NO at low temperature. On one hand, carbon-supported catalysts are reported to be resistant, even promoted, in gases containing 100–1000 ppm $SO_2$ at temperatures lower than 423 K [12–14], while it is well known that titania-supported vanadia is deactivated by $SO_2$ at temperatures lower than 623 K [17]. In future works the resistance of our catalyst against $SO_2$ will be tested. On the other hand, due to the high surface area of carbon, this can carry more dispersed vanadium per support weight than other supports with less surface area. The more vanadium can be dispersed in a support, the less amount of catalyst will be needed for a certain process that entails reduction in cost of catalyst and energy. Simple calculations confirm that the amount of vanadia loaded at monolayer coverage in our carbon is comparable to that on titania. The nominal $VO_x$ surface density at monolayer coverage (6 wt%) of our carbon is 1.16 V nm$^{-2}$ (Table 2) which is lower than that in other oxide supports, viz. $\sim 7$ V nm$^{-2}$ [1]. Despite this, the surface area of this carbon (617 m$^2$/g) is much higher than the surface area of other oxide supports. Assuming an anatase support with very high surface area, e.g., 100 m$^2$/g, the total amount of vanadium loaded at monolayer coverage will be 1.16 mmol/g of support while in our carbon it is 1.20 mmol/g.

Consequently, the total amount of active sites, i.e., surface vanadium species, on our carbon support is slightly higher than that on a traditional oxide support as $TiO_2$. The achievement of higher vanadium loadings at monolayer coverage is envisaged as feasible in our carbon support. To meet this objective, the surface area and also the number of hydroxyl surface groups of this carbon can be increased. For instance, the hydroxyl groups of this carbon can be maximized by additional oxidative treatments in $HNO_3$.

## 5. Conclusions

A monolithic catalyst based on vanadium supported on mesoporous carbon has been prepared. This catalyst had activities and selectivities comparable to those reported in the literature for the SCR of NO with $NH_3$ at low temperatures. It was possible to determine the morphology of this novel catalyst by using different techniques, viz. atomic force microscopy, $N_2$ physisorption, and XRD. AFM was very informative for the characterization of catalyst crystallites. Vanadium is supported on our carbon-coated monoliths as $V_2O_5$ overlayers up to around 6 wt% loading. Above this loading vanadia crystallites appear. The exposure of vanadium, i.e., dispersion, and the structure of vanadium turned out to be the determinant of activity and selectivity, respectively. Both activity and selectivity to $N_2$ drop dramatically for loadings surpassing that of monolayer coverage.

The turnover frequency of our carbon-supported catalyst is lower than that of titania-supported catalyst but higher than that of alumina- and silica-supported catalysts. In contrast with oxide-supported catalysts, the specific activity of our catalyst (TOF) is constant below monolayer coverage, regardless of the loading.

Despite that carbon-supported vanadia exhibits lower specific activity than titania-supported vanadia, the former shows some advantages that make carbon a promising support for SCR at low temperature. Carbon-supported vanadia is not deactivated by $SO_2$ at low temperatures while titania-supported vanadia is readily deactivated by $SO_2$. Moreover, the much higher surface area of carbon and the possibility of maximing the hydroxylation enables it to disperse a higher amount of active phase per weight of support than titania.

## Acknowledgments

The authors thank Hüttenes-Albertus (Hannover) and Corning (New York) for supplying the Furan resin and cordierite monoliths, respectively. The authors are indebted to the Spanish Ministry of Science and Technology (PPQ-2002-02698 and BFM-2001-0209) and Diputacion General de Aragón for the financial support. E. García-Bordejé acknowledges the MCyT for a Ramón y Cajal contract.

## References

[1] I.E. Wachs, B.M. Weckhuysen, Appl. Catal. A 157 (1997) 67.
[2] G. Deo, I.E. Wachs, J. Haber, Crit. Rev. Surf. Chem. 4 (1994) 141.
[3] G. Bond, S.F. Tahir, Appl. Catal. (1991) 1.
[4] M.A. Bañares, Catal. Today 51 (1999) 319.
[5] I.E. Wachs, G. Deo, B.M. Weckhuysen, A. Andreini, M.A. Vuurman, M. de Boer, M.D. Amiridis, J. Catal. 161 (1996) 211.
[6] I.E. Wachs, Catal. Today 27 (1996) 437.
[7] H. Eckert, I.E. Wachs, J. Phys. Chem. 93 (1989) 6796.
[8] B.M. Weckhuysen, D.E. Keller, Catal. Today 78 (2003) 25.
[9] G. Centi, Appl. Catal. A 147 (1996) 267.
[10] K. Inumaru, M. Misono, T. Okuhara, Appl. Catal. A 149 (1997) 133.
[11] S. Kasaoka, E. Sasaoka, I. Iwasaki, Bull. Chem. Soc. Jpn. 62 (1989) 1226.
[12] Z. Zhu, Z. Liu, H. Niu, S. Liu, J. Catal. 187 (1999) 245.
[13] Z. Zhu, Z. Liu, S. Liu, H. Niu, T. Hu, T. Liu, Y. Sie, Appl. Catal. B 26 (2000) 25.
[14] Z. Zhu, Z. Liu, S. Liu, H. Niu, Appl. Catal. B 30 (2001) 267.
[15] T. Valdes-Solis, G. Marbán, A.B. Fuertes, Appl. Catal. B 46 (2003) 261.
[16] E. García-Bordejé, L. Calvillo, M.J. Lázaro, R. Moliner, R., Appl. Catal. B, in press.
[17] H. Bosch, F. Janssen, Catal. Today 2 (1988) 369.
[18] M. Inomata, A. Miyamoto, Y. Murakami, J. Catal. 62 (1980) 140.
[19] F. Janssen, F. van der Kerkhof, H. Bosch, J.R.H. Ross, J. Phys. Chem. 91 (1987) 5921.

[20] T. Grzybek, H. Papp, Appl. Catal. B 1 (1992) 271.
[21] J. Pasel, P. Kasner, M. Gazzano, A. Vaccari, W. Makowski, T. Lojewski, R. Dziembaj, H. Papp, Appl. Catal. B 18 (1998) 199.
[22] T. Grzybek, J. Pasel, H. Papp, Phys. Chem. Chem. Phys. 1 (1999) 341.
[23] G. Marbán, R. Antuña, A.B. Fuertes, Appl. Catal. B 41 (2003) 323.
[24] T. Valdés-Solís, G. Marbán, A.B. Fuertes, Catal. Today 69 (2001) 259.
[25] T. Vergunst, M.J.G. Linders, F. Kapteijn, J.A. Moulijn, Catal. Rev.-Sci. Eng. 43 (2001) 291.
[26] E. García-Bordejé, F. Kapteijn, J.A. Moulijn, Carbon 40 (2002) 1079.
[27] J.A. Moulijn, A. Tarfaoui, F. Kapteijn, Catal. Today 11 (1991) 1.
[28] L.K. Doraiswamy, M.M. Sharma, Gas-Solid and Solid-Solid Reactions, vol. 1, Wiley, New York, 1984, Chap. 3.
[29] L.R. Radovic, F. Rodriguez-Reinoso, in: Carbon Materials in Catalysis, in: Chemistry and Physics of Carbon, vol. 25, Dekker, New York, 1997, p. 243.
[30] J. Haber, M. Witko, R. Tokarz, Appl. Catal. A 157 (1997) 3.
[31] A. Da Costa, C. Mathieu, Y. Barbaux, H. Poelman, G. Dalmai-Vennik, L. Fiermans, Surf. Sci. 370 (1997) 339.
[32] J. Marangozis, Ind. Eng. Chem. Res. 31 (1992) 987.
[33] G. Marbán, A.B. Fuertes, Catal. Lett. 84 (2002) 13.
[34] F. Kapteijn, L. Singoredjo, N.J.J. Dekker, M.A. Moulijn, Ind. Eng. Chem. Res. 32 (1993) 445.
[35] A. Miyamoto, Y. Yamazaki, M. Inomata, Y.J. Murakami, J. Phys. Chem. 85 (1981) 2366.
[36] N.-Y. Topsoe, J.A. Dumesic, H. Topsoe, J. Catal. 151 (1995) 241.
[37] U.S. Ozkan, Y. Cai, M. Kumthekar, Appl. Catal. A 96 (1993) 365.
[38] V.I. Parvulescu, S. Boghosian, V. Parvulescu, S.M. Jung, P. Grange, J. Catal. 217 (2003) 172.
[39] M.D. Amiridis, I.E. Wachs, G. Deo, J.M. Jehng, D.S. Kim, J. Catal. 161 (1996) 246.
[40] L. Lietti, G. Ramis, F. Berti, G. Toledo, D. Robba, G. Busca, P. Forzatti, Catal. Today 42 (1998) 101.
[41] A. Andreini, M. De Boer, M.A. Vuurman, G. Deo, I.E. Wachs, J. Chem. Soc., Faraday Trans. 92 (1996) 3267.
[42] A. Baiker, B. Handy, J. Nickl, M. Schraml-Marth, A. Wokaun, Catal. Lett. 14 (1992) 89.